

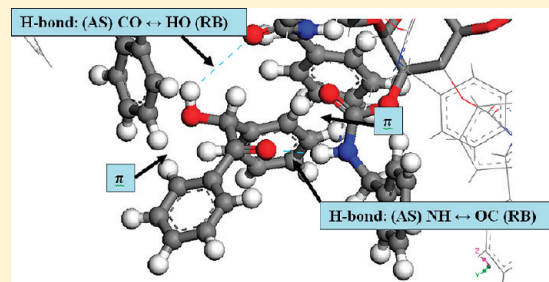
Infrared Spectroscopy and Molecular Simulations of a Polymeric Sorbent and Its Enantioselective Interactions with Benzoin Enantiomers

Hung-Wei Tsui, Jonathan N. Willing, Rahul B. Kasat,[†] Nien-Hwa Linda Wang, and Elias I. Franses*

School of Chemical Engineering, Purdue University, 480 Stadium Mall Drive, West Lafayette, Indiana 47907-2100, United States

Supporting Information

ABSTRACT: Retention factors, k_R and k_S , and enantioselectivities, $S \equiv k_R/k_S$, of amylose tris[(S)- α -methylbenzylcarbamate] (AS) sorbent for benzoin (B) enantiomers were measured for various isopropyl alcohol (IPA)/*n*-hexane compositions of the high-performance liquid chromatography (HPLC) mobile phase. Novel data for pure *n*-hexane show that $k_R = 106$, $k_S = 49.6$, and $S = 2.13$. With some IPA from 0.5 to 10 vol %, with $S = 1.8$ –1.4, the retention factors were smaller. Infrared spectra showed evidence of substantial hydrogen bonding (H-bonding) interactions in the pure polymer phase and additional H-bonding interactions between AS and benzoin. Density functional theory (DFT) was used to model the chain–chain and chain–benzoin H-bonding and other interactions. DFT was also used to predict fairly well the IR wavenumber shifts caused by the H-bonds. DFT simulations of IR bands of NH and C=O allowed for the first time the predictions of relative intensities and relative populations of H-bonding strengths. Molecular dynamics (MD) simulations were used to model a single 12-mer polymer chain. MD simulations predicted the existence of various potentially enantioselective cavities, two of which are sufficiently large to accommodate a benzoin molecule. Then “docking” studies of benzoin in AS with MD, Monte Carlo (MC), and MC/MD simulations were done to probe the AS–B interactions. The observed enantioselectivities are predicted to be primarily due to two H-bonds, of the kind AS CO \cdots HO (*R*-benzoin) and AS NH \cdots OC (*R*-benzoin), and two π – π (phenyl–phenyl) interactions for (*R*)-benzoin and one H-bond, of type AS CO \cdots HO (*S*-benzoin), and one π – π interaction for (*S*-benzoin). The MC/MD predictions are consistent with the HPLC and IR results.



1. INTRODUCTION

Polysaccharide (PS)-based sorbent materials, or chiral stationary phases (CSPs), especially derivatized amylose and cellulose polymeric CSPs, developed by Okamoto and Yashima,¹ have been used widely for most analytical and preparative chiral separations of low molecular weight compounds.² Kasat et al.^{3,4} have studied the chiral discrimination of amylose tris-(3,5-dimethylphenylcarbamate), or ADMPC, or AD, and cellulose tris-(3,5-dimethylphenylcarbamate), or CDMPC, or CD, which have the same side chain and a different backbone. This article focuses on another widely used amylose-based CSP, amylose tris[(S)- α -methylbenzylcarbamate], or AS-MBC, or simply AS (Figure 1). It has an amylose backbone, as does AD, but a different side chain. A comparison between AS and AD may help elucidate further the mechanisms of chiral discrimination in this class of sorbents. A similar theme is shown here for benzoin with AS.

Kasat et al.⁵ used attenuated total reflection infrared spectroscopy (ATR-IR), X-ray diffraction (XRD), cross-polarization/magic-angle spinning (CP/MAS), MAS solid-state nuclear magnetic resonance (NMR) spectroscopy, and density functional theory (DFT) to study molecular environments in the polymers AD, CD, and AS. They concluded that AS has the same backbone helical pitch length as AD. The side chains of AS have nonplanar

conformations, which imply a shorter distance between polymer chains than in AD. They also reported the behavior of AD upon interacting with different solvents.⁶ By using molecular mechanics (MM) and molecular dynamics (MD) simulations, with an 8-mer polymer rod model having a 4-fold helix, they inferred that the polymer rods contain many nanometer-sized cavities with intrarod hydrogen bonds, H-bonds. Upon interacting with polar solvents, the polymer crystallinity and the side-chain mobility increase, and the distribution of strengths of the H-bonding states of AD changes significantly.

Kasat et al.⁷ studied the key interactions of phenylpropanolamine (PPA) with AD, CD, and AS. The enantioselectivities were quite different. AD showed high enantioselectivity, $S \equiv k_R/k_S = 2.4$, where k_R and k_S are the retention factors of the *R* and *S* enantiomers. AS showed no enantioselectivity ($S \approx 1.0$). CD had the reverse elution order and a low enantioselectivity ($S = 0.8$). Their ATR-IR results indicated that PPA causes different changes in hydrogen bonding of amide groups of these polymers. They concluded that the enantioselectivity of AD for PPA is due to

Received: July 10, 2011

Revised: September 19, 2011

Published: September 26, 2011

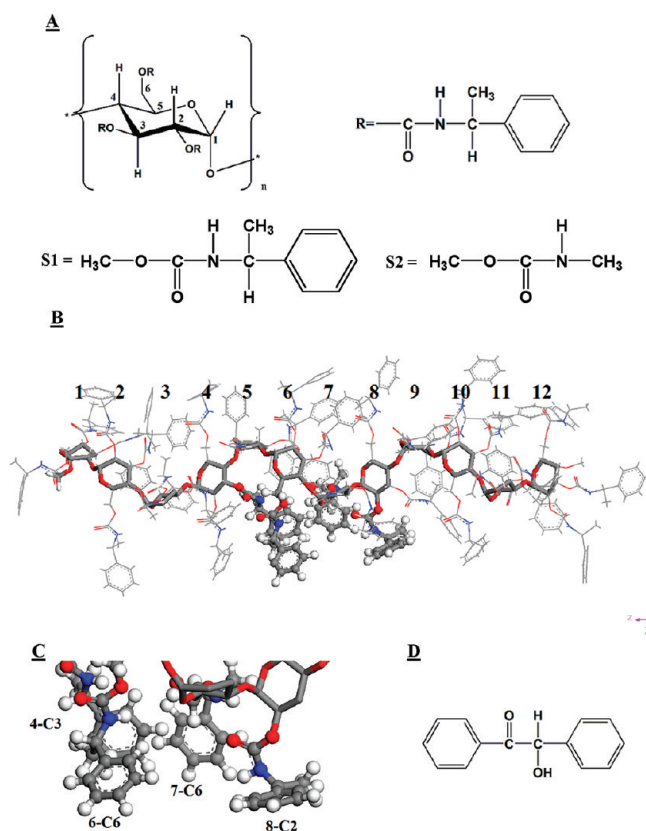


Figure 1. (A) Molecular structure of the polymer repeat unit of the AS polymer, with R being the side chain; S1 and S2 (or MMC) are the side-chain models. (B) Molecular mechanics 3D model of the molecular structure of a model with 3 unit cells and 12 monomer units. Amylose backbone atoms are shown in stick representation, and side chains are shown in line representation. The cavity A used for docking studies is shown with a ball-and-stick representation. (C) Detail of panel B showing cavity A formed by the following four side chains: chain C3 of monomer 4, chain C6 of monomer 6, chain C6 of monomer 7, and chain C2 of monomer 8. The cavity, shown in ball-and-stick representation, is used for docking studies. (D) Molecular structure of benzoin (the trans conformation is shown).

differences in the formation of H-bonds and in $\pi-\pi$ (phenyl–phenyl) interactions between the sorbent and the solute.

Wirz et al.⁸ used polarization modulation ATR-IR spectroscopy with hexane in a flow cell and DFT calculations to study the chiral discrimination of ethyl lactate with AS. They concluded that C=O groups of the (R)-ethyl lactate enantiomer form stronger hydrogen bonds with the polymer NH groups than those of (S)-ethyl lactate. Such interactions were deemed to be crucial for enantioselectivity. Wirz et al.⁹ also used a combination of high-performance liquid chromatography (HPLC), and ATR-IR to probe changes in the H-bonding states of AS with pantothenate in 20 vol % isopropyl alcohol (IPA) in cyclohexane. Although no specific values of S were reported, the authors concluded that their observed enantioselectivity is due to stronger hydrogen bonding between (R)-pantothenate C=O groups and AS NH groups than those of (S)-pantothenate.

Cass and co-workers^{10,11} reported a range of enantioselectivities of various chiral sulfoxides and N-arylamides, which have no asymmetric carbons but planar-torsion-based chiral centers. They used several PS-based CSPs, including AD and AS. The reported

enantioselectivities were found, as expected, to depend on the type of polysaccharide backbone and side chain and the type and composition of the mobile phase. For a series of amylose-based CSPs, Booth et al.¹² concluded that the chirality of the amylose backbone affected the elution order and that the chirality of the carbamate side chain affected the value of the enantioselectivity. Hu and Jiang¹³ used molecular simulations to model the flow and enantioseparation of phenylglycine enantiomers.

In a series of pioneering papers with AD, Wang and co-workers^{14–17} reported that the retention factors depend on the type and composition of the alcohol modifier in the mobile phase. The elution order could be reversed sometimes when different types of alcohol modifiers were used. The alcohol modifier may change conformations and steric environments of the polymer cavities, the properties of which were considered to be important for the enantioselectivities. Ma et al.¹⁸ also reported that the polarity of the mobile phase may lead to conformational changes of the sorbent. In certain cases, a reversal of the elution order could be observed by changing the composition of certain hexane/alcohol mixtures. The idea of the chiral cavities being mostly relevant to the enantioselectivity was recently used for molecular simulations studies, or “docking” studies.^{3,4,19} Li et al.¹⁹ used an AD polymer rod model to investigate the enantioselectivity of metalaxyl and benalaxyl enantiomers. No spectroscopic data are available for these systems. They concluded that the predicted energy differences of the complexes of sorbent/(R)-solute and sorbent/(S)-solute are due to differences in hydrogen bonding between the enantiomers and sorbent sites in the cavities.

In a screening study of enantioselectivities of AS for various solutes at 25 °C in 10 vol % IPA/n-hexane, we found that the enantioselectivity for benzoin (B) was quite high ($S = 1.8$, see section 3.1), and higher than those of several similar molecules, such as ethyl lactate, methyl mandelate, 1-phenyl-1-propanol, 1-phenyl-2-propanol, 2-phenyl-1-propanol, 2-amino-1,2-diphenylethanol, and others. For this reason, benzoin was chosen for systematic mechanistic study, and it is the main focus of this article. Benzoin is a simple model molecule with only a few functional groups: C=O, OH, and phenyls. The OH group allows for easier IR probing of the state of solute in contact with the polymer, as shown below. Okamoto et al.²⁰ had reported values of $k_S = 4.29$, $k_R = 8.49$, and $S = 1.98$ for a homemade column of AS with benzoin at 25 °C, in a 10 vol % IPA/n-hexane solvent. Muthupandi et al.²¹ also reported retention times of $t_S = 8.533$ and $t_R = 13.350$ min for the S and R enantiomers in 15 vol % IPA in “hexanes”, which is a mixture of hexane isomers. Retention factors or S-values were not reported.

In section 3.1, we report HPLC data for various concentrations of IPA in the n-hexane mobile phase. We present for the first time, to our knowledge, HPLC data with pure n-hexane. These data are important, to allow more direct comparisons of the data with enantioselectivities predicted with two-component polymer/solute simulations. It has been established from XRD and IR that, unlike hexane/alcohol mixtures, hexane does not change the H-bonding state of the polymer.⁶ The new IR data allow the probing of the solute H-bonding state, since benzoin contains an OH group, which was modified to an OD group. The IR band of OD is shifted to an empty spectral zone. We present DFT simulation predictions not only of wavenumbers but also of relative intensities. This allows quantitative prediction of the relative populations of different H-bonding states of the NH and C=O groups of AS. Such predictions allow unique insights in the

AS molecular structure and comparisons to prediction of MD simulations.

In this article, we present MD simulations with various force fields for comparison. Even more importantly, we present novel results of Monte Carlo (MC) and MC/MD docking simulations. The latter simulations have a higher predictive value than the MD simulations, because the locations of the solute in the chiral cavity are chosen without bias.

2. MATERIALS AND METHODS

2.1. Materials. AS-polymer-coated silica beads, or ChiralPak AS, and semipreparative ChiralPak AS columns, which were 100 mm long with a 10 mm column diameter and 20 μm particle diameters, were provided by Chiral Technologies (Exton, PA). HPLC-grade 2-propanol, or isopropyl alcohol (IPA), was purchased from Mallinckrodt Chemicals (Phillipsburg, NJ). HPLC-grade *n*-hexane was purchased from EMD Chemicals (Gibbstown, NJ). 1,3,5-Tributylbenzene (TTBB), benzoin racemate (B), (*R*)-benzoin (R-B), (*S*)-benzoin (S-B), carbon tetrachloride, tetrahydrofuran (THF), and methanol-OD were purchased from Sigma-Aldrich (Milwaukee, WI).

Deuterated benzoin racemate (B-OD) was synthesized with a H to D exchange reaction, by dissolving B-OH racemate, or each of the enantiomers, in methanol-OD in a molar ratio of 3:100. The solution was stirred for at least 3 h at 25 °C.²² The resulting mixture contained about 25 mol % B-OD and 75 mol % B-OH.

2.2. HPLC Apparatus and Procedures. An Agilent 1100 HPLC apparatus was used. It consisted of a micro vacuum degasser, a built-in variable-wavelength detector (VWD) with wavelengths ranging from 950 to 190 nm, an autosampler, and a thermostated column compartment for controlling the column temperature within 1 °C in the range from 25 to 80 °C. A binary pump was used to control the flow rate from 0.1 to 5 mL/min at 25 °C. Usually a flow rate of 1.0 mL/min was used. The mobile phase was a mixture of IPA and *n*-hexane. The pulse injection volume was 20 μL . The retention time of a nonadsorbing solute, TTBB, ($t_{\text{ref}} = 5.5$ min) was used as a reference. The retention factors, k_R and k_S , of the benzoin enantiomers were found from the standard equation

$$k_i \equiv \frac{(t_i - t_{\text{ref}})}{t_{\text{ref}}}$$

where $i = R$ or S .

Solute mass balances, for experiments with and without the column, confirmed that no benzoin was retained in the column after the elution.

2.3. IR Spectroscopy Apparatus and Procedures. A Nicolet Protégé 460 Fourier transform infrared spectrometer, equipped with a mercury–cadmium–telluride (MCT) detector cooled with liquid nitrogen, was used to obtain all IR spectra. The spectral contributions from water vapor and carbon dioxide were minimized by continuously purging the instrument's sample chamber with dry air from a Balston purge gas generator. ATR spectra were collected with unpolarized incident light at 298 K by use of a custom-made accessory with a Si-ATR plate (Wilmad, NJ). The incident angle was typically 50°, with seven reflections. All spectra were taken at intervals of about 1 cm^{-1} with Happ-Genzel apodization. The resolution and reproducibility are estimated to be better than $\pm 0.2 \text{ cm}^{-1}$. Even though the Si-ATR plates have an absorption cutoff at about 1500 cm^{-1} , reliable spectra were obtained down to 1000 cm^{-1} by subtraction

of the blank spectrum. For enhancing the spectral accuracy and the signal/noise ratio, the spectra were averaged by collecting 256 scans.

The polymer was obtained from coated polymer beads by dissolving the beads in THF and separating the solutes from the silica particles by filtration. The THF solution was deposited on the ATR plates and then dried. The films were annealed in a vacuum oven for at least 1 h at 80 °C. Spectra of dry-cast films were obtained first. Then benzoin solutions in carbon tetrachloride were deposited on the AS films, and the CCl₄ was allowed to evaporate for at least 20 min.

2.4. Computational Methodology. **2.4.1. Density Functional Theory Simulations.** The Gaussian 03 program was used for the electronic structure calculations. The hybrid B3LYP (Becke, three-parameter, Lee–Yang–Parr) functional with the 6-311+g(d,p) basis set (triple- ζ level) was used. This functional yields similarly accurate predictions of energies, intermolecular geometries, and vibrational frequencies as those obtained by using the ab initio MP2 (Møller–Plesset perturbation theory) method. It includes a combination of Hartree–Fock exchange with a DFT exchange–correlation. The basis set includes polarization functions on hydrogen and other atoms and diffuse functions with diffuse sp shells for other atoms. The calculations were done for (a) benzoin; (b) a model AS side chain, termed “S1” (it has 26 atoms); and (c) a simplified model of the side chain, “S2” (it has 13 atoms), which is the same as the molecule methyl N-methylcarbamate (MMC); see Figure 1. The structures and energies of these side chains at minimum energies were obtained within about 2 days of computations on a personal computer. The IR wavenumbers and intensities of B, S1, and S2 were obtained for the optimized structures. A correction factor of 0.96 for all predicted wavenumbers was used.⁷ Predictions of wavenumber shifts are generally considered to be more accurate than predictions of absolute wavenumbers.

To estimate the strengths of H-bonded interactions between the side chains in the actual polymer phase, two chains in contact were modeled with DFT. For probing H-bond energies and IR wavenumbers of interacting chains, computations for a pair of side chains S1–S1 took too long. To reduce the computation time, computations were done for a simpler S2–S2 pair, which has fewer steric hindrance effects. The interactions between R-B or S-B and a single chain were modeled with DFT with either an S1 or an S2 chain. Each of these computations took about 2 weeks and 1 week, respectively. Although each of these calculations may not always lead to a configuration of global minimum energy, they provided some useful predictions.

2.4.2. Molecular Dynamics and Monte Carlo Computations. Since it was inferred from XRD that AS has the same pitch length as AD, which forms a 4-fold helix,²³ a 12-mer (three unit cells of four monomers each) model of the AS backbone was constructed first. The Linked-Atom Least-Squares (LALS) package was used. The pitch length was chosen to be 1.46 nm, as found from XRD.⁷ The energy of the resulting polymer (981 atoms; see Figure 1), which has the shape of a rod with attached side chains, was first minimized by molecular mechanics (MM) simulations with the Discover module from the Materials Studio Modeling software (Accelrys), version 5.0. For finding the global minimum more reliably, MD simulations with the same module were used. The consistent-valence force field (CVFF) was mostly used in both the MM and the MD simulations.²⁴ Some comparisons with some other force fields were made. The CVFF force field uses a Morse potential for modeling bond stretching, Coulomb's law

for electrostatic interactions, and a Lennard-Jones function for van der Waals (vdW) interactions. Hydrogen-bonding interactions are modeled as a combination of electrostatic and vdW interactions. With these features, the models may lead to somewhat accurate predictions of the molecular structures but less accurate predictions of the H-bond energies and the IR wavenumber shifts.²⁴

To explore as much as possible the potential energy surface and allow the calculations to reach as closely as possible the “equilibrium” minimum-energy configuration by avoiding energy barriers, the MD simulations were done as follows. An NVT (number/volume/temperature) ensemble controlled by a Nose-Hoover thermostat was used,²⁵ with a time step of 1 fs. Simulations were first done at 500 K for 1 ns; then at 450 K for 1 ns; then at 350 K for 1 ns; and finally at 298 K for 3 ns. The formation of hydrogen bonds was recognized from the range of distances d between H and X and the angles θ between X–H and H \cdots Y, X–H \cdots Y.

For docking studies, the above 12-mer polymer model was used. For AS, AD, or CD, Kasat et al.⁷ also used a 12-mer. For AD, Li et al.¹⁹ used a 36-mer. In this article, we focus on the central section of the 12-mer, containing monomers 5–8, to minimize possible chain end effects. In this section, there were cavities of sufficient size to accommodate one benzoin molecule.

The next step is the selection of the docking method. MD was used previously by our group to probe enantioselective interactions of AS, AD, and CD with PPA.⁷ In this method, one suitable cavity is chosen at a time, and the solute molecule is inserted with some initial orientation, as suggested by the IR-inferred interactions. Then the MD program from Materials Studio is run until it reaches equilibrium, and the resulting interactions are identified and interpreted. Some bias in selection of the cavities and initial orientations may result in missing the detection of possible lower energy minima. For this reason, the second method, MC-docking simulations, was also used for comparison. The Sorption module from Materials Studio was used for calculating the energies of each configuration. In this MC method, the whole polymer section of monomers 5–8 was used in searching for possible docking sites, without the above bias. Since the structure of AS would not change much after the equilibration, one instant frame of the AS structure was randomly chosen from the configurations around the equilibrium state. During the simulations, the structures of the AS and the benzoin molecule were fixed, to search for the strongest interaction sites along the surfaces of the AS cavities. van der Waals forces at distances of 0.5 nm or less were considered, to compensate for a possible overestimation of the π – π interactions with CVFF and to improve the efficiency of searching for the binding sites. The simulations were performed with five temperature cycles, 10^5 maximum loading steps, and 10^7 production steps. The annealing search was automatically controlled by the program. At the end of the simulations, 20 frames with the lowest minimum energies were chosen as representing the most likely configurations.

Even though it is more likely to find the global energy minimum with the MC than with the MD method, both methods were used, and the results are compared. Moreover, MC followed by MD was also used for comparison. In this “hybrid” method, the results of the solute and chain orientations and the configurations from the MC searching simulations were set as the initial values for subsequent MD simulations. Since polymer–polymer and polymer–solute interactions are not considered

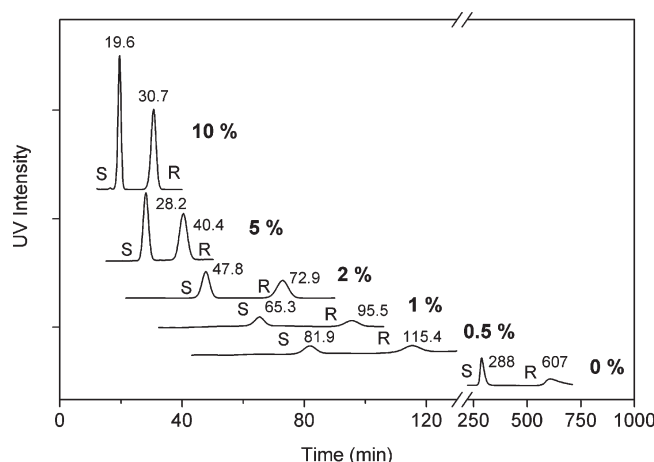


Figure 2. HPLC results for retention times of (S)- and (R)-benzoin enantiomers with ChiralPak AS beads for various concentrations of IPA in *n*-hexane (vol %) at 25 °C.

Table 1. Retention Factors and Enantioselectivities of Benzoin Enantiomers with AS Polymer^a

% IPA	k_R	k_S	S
10	4.62	2.58	1.79
5.0	6.35	4.13	1.54
2.5	12.3	7.69	1.59
1.0	16.4	10.87	1.51
0.5	19.6	13.62	1.44
0	106	49.6	2.13

^a Retention factors (k_R and k_S) and enantioselectivities (S) were measured for different vol % IPA in *n*-hexane at 25 °C; see Figure 2. The retention time of a nonadsorbing reference molecule, TTBB, was 5.5 min under the same conditions.

in these simulations, one may expect a qualitative agreement with enantioselectivity data or, at best, a semiquantitative agreement.

3. RESULTS AND DISCUSSION

3.1. HPLC Results for Effects of Solvent Composition on Retention Factors and Enantioselectivities. Retention times and retention factors of (R)-benzoin (R-B) and (S)-benzoin (S-B) increase as the IPA concentration decreases from 10% to 0.5% (Figure 2 and Table 1). This trend is generally expected, because as the solvent becomes less polar, the solute H-bonding functional groups interact more with the polar sorbent and have less competition from the OH groups of IPA. The values of the enantioselectivity S decrease from about 1.8 to about 1.4, and the enantiomer peaks are well separated.

The retention factors reported here for 10% IPA in *n*-hexane mobile phase differ from those previously reported by Okamoto et al.²⁰ by 70–80%. The difference may be due to the use of different columns with different loading of polymer per unit volume of the column. Their reported enantioselectivity S of 1.98 differs less from our data (1.79).

For pure *n*-hexane as the mobile phase, the retention times and factors are much higher. Evidently benzoin binds much more strongly to AS, because it does not form H-bonds with hexane. The hexane does not change the sorbent H-bonding state, as

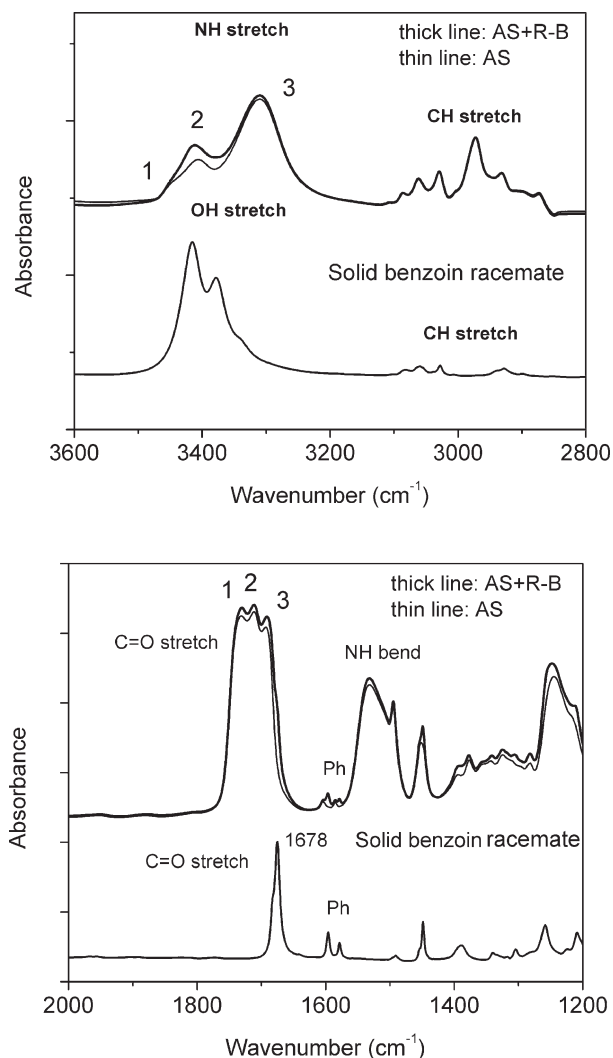


Figure 3. ATR-IR spectra of pure AS and of AS upon equilibration with (*R*)-benzoin in CCl_4 and evaporation of CCl_4 ; also shown is the spectrum of solid benzoin racemate. The range between 2800 and 2000 cm^{-1} has no peaks and is not shown. The scales in the top ($3600\text{--}2800\text{ cm}^{-1}$ range) and the bottom ($2000\text{--}1200\text{ cm}^{-1}$ range) panels are different, for convenience in observing. The phenyl and methyl CH bands for AS and AS + R-B overlap. At this scale, the spectrum of AS + S-B looks similar to that of AS + R-B and is not shown. For the difference spectra (AS + R-B) – AS and (AS + S-B) – AS, see Figure 6.

determined from IR and from XRD spacings.⁶ It can be argued that the AS H-bonding interactions do not change in the presence of *n*-hexane. The enantioselectivity value of $S = 2.13$ suggests that (*R*)-benzoin interacts with AS more strongly than (*S*)-benzoin. (*R*)-Benzoin either forms one H-bond which is much stronger than that of (*S*)-benzoin or it forms an additional H-bond. The IR results below suggest that the latter possibility is more likely.

3.2. Attenuated Total Reflection IR and Density Functional Theory Results for Interactions between Benzoin Enantiomers and AS Polymer. 3.2.1. *ATR-IR Spectra of AS, Benzoin, and AS/Benzoin Enantiomer Systems.* IR spectra of AS before and after absorption of R-B are shown in Figure 3; the spectrum of the benzoin racemate is also shown for comparison. The assignments will be discussed first, followed in section 3.2.2

Table 2. DFT Predictions of Wavenumbers and Intensities of Certain IR Bands of Model Side Chains S1 and S2 and of Benzoin.^a

system	molecule	band	ν_1 , cm^{-1}	experiment, cm^{-1}	I	comment
1	S1	$\text{NH} _{\text{s}}$	3495	<i>b</i>	39	no H-bond
2	S2	$\text{NH} _{\text{s}}$	3499	3460, ²⁶ 3474 ²⁷	41	no H-bond
3	S1	$\text{C}=\text{O} _{\text{s}}$	1702	<i>b</i>	402	no H-bond
4	S2	$\text{C}=\text{O} _{\text{s}}$	1713	1735, ²⁶ 1737 ²⁷	399	no H-bond
5	S1	$\text{NH} _{\text{b}}$	1471	<i>b</i>	373	no H-bond
6	S2	$\text{NH} _{\text{b}}$	1508	1525, ²⁶ 1520 ²⁷	253	no H-bond
7	S1	$\text{Ph} _{\text{s}}$	1572	1604	4	<i>b</i>
8	S1	$\text{Ph} _{\text{s}}$	1553	1585	2	<i>b</i>
9	$\text{B} _{\text{trans}}$	$\text{OH} _{\text{s}}$	3692	<i>b</i>	57	no H-bond
10	$\text{B} _{\text{trans}}$	$\text{C}=\text{O} _{\text{s}}$	1656	<i>b</i>	196	no H-bond
11	$\text{B} _{\text{trans}}$	$\text{Ph} _{\text{s}}$	1576	1596	8	<i>b</i>
12	$\text{B} _{\text{trans}}$	$\text{Ph} _{\text{s}}$	1570		35	<i>b</i>
13	$\text{B} _{\text{trans}}$	$\text{Ph} _{\text{s}}$	1557	1578	1	<i>b</i>
14	$\text{B} _{\text{trans}}$	$\text{Ph} _{\text{s}}$	1551		13	<i>b</i>
15	$\text{B} _{\text{cis}}$	$\text{OH} _{\text{s}}$	3525	3474 ²⁷	106	intra H-bond
16	$\text{B} _{\text{cis}}$	$\text{C}=\text{O} _{\text{s}}$	1626	1684 ²⁷	182	intra H-bond

^a A scaling factor of 0.96 was used for all frequencies. ^b Not available.

by a more detailed spectral analysis and interpretation of certain key bands.

The NH-stretching band of the side chains indicates three peaks. Peak 1 is a “shoulder” at ca. 3449 cm^{-1} . Peaks 2 and 3 overlap and have wavenumbers of ca. 3407 and 3310 cm^{-1} . Hence, there are three populations of NH groups. Peaks 2 and 3 correspond to medium and strongly H-bonded groups. Peak 1 corresponds to either weakly H-bonded or non-H-bonded groups. The NH-stretching band of a similar molecule, methyl *N*-methylcarbamate or MMC (or the model side chain S2), in the gas phase, where it is expected to be non-H-bonded, has one peak at 3460 cm^{-1} in one reference²⁶ or 3474 cm^{-1} in another reference.²⁷ Hence peak 1 at 3449 cm^{-1} is more likely to arise from non-H-bonded groups. DFT calculations support this inference, predicting NH stretch wavenumbers of 3499 cm^{-1} for non-H-bonded chain S2 or MMC and 3495 cm^{-1} for non-H-bonded chain S1 (Table 2).

The bands at ca. $3100\text{--}2850\text{ cm}^{-1}$ are due to CH stretches of the phenyl and CH_3 groups. Since they overlap with some benzoin bands and do not change much upon absorption of benzoin, they are not thought to provide sensitive structural information, and they are not considered further. The amide I band, which is due mostly (ca. 80%) to $\text{C}=\text{O}$ stretching,²⁸ is quite broad and shows three overlapping peaks at ca. 1732 , 1711 , and 1693 cm^{-1} . They indicate three populations of H-bonded $\text{C}=\text{O}$ groups: free or weakly H-bonded groups (peak 1), medium H-bonded groups (peak 2), and strongly H-bonded groups (peak 3). The non-H-bonded $\text{C}=\text{O}$ band of MMC (Figure 1), which appears at 1735 cm^{-1} , is the basis for this inference. The DFT calculations predict that the wavenumber of the non-H-bonded $\text{C}=\text{O}$ stretch band of MMC should be at 1713 cm^{-1} (Table 2), which is within 2% of the data. Since the third peak overlaps with the $\text{C}=\text{O}$ peak of benzoin at 1675 cm^{-1} , the use of difference spectra is needed (see below). Both the NH and $\text{C}=\text{O}$ stretch bands change upon the absorption of benzoin, indicating that the benzoin is incorporated into or dissolved in

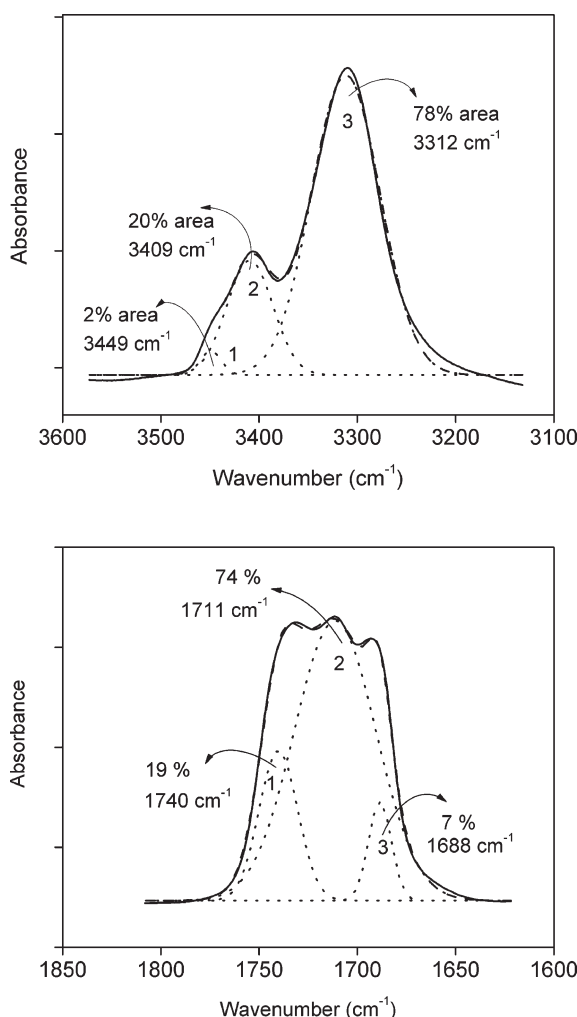


Figure 4. Deconvolution of (top) NH stretching band and (bottom) amide I band in the ATR-IR spectrum of dry AS polymer. The wavenumbers and area percentages of these peaks are indicated. The fit is good; $R^2 = 0.996$ (top) and 0.999 (bottom).

the polymer structure and that the polymer H-bonding state changes upon interaction of sorbent with benzoin. The amide II, or NH-bending (60%) and CN (40%) stretching band,²⁸ at ca. 1532 cm^{-1} , is quite strong and broad, and it shows some changes upon benzoin absorption (Figure 3). The band at 1495 cm^{-1} corresponds to a phenyl C–C vibration. The amide III band at 1245 cm^{-1} arises from many complex vibrations and is not analyzed further.

The bands at 1604 and 1585 cm^{-1} (see Figure 3) are assigned to the symmetric and asymmetric C–C stretching vibrations of the AS phenyl groups.^{5,29} These assignments are based on DFT simulations (7 and 8 in Table 2). As reported, the phenyl C–C stretching bands of AS are weak, because no polar group is directly attached to the phenyl groups, resulting in small instantaneous dipole moments during the vibration.⁵ Because these bands do not overlap with the respective phenyl C–C stretching bands of benzoin (which appear at 1596 and 1578 cm^{-1}), they are used to normalize the AS and B spectra in the determination of the difference spectra. The DFT wavenumber predictions are quite accurate, to within 2% of the data.

The wavenumber of non-H-bonded OH groups ranges normally from 3600 to 3400 cm^{-1} . The wavenumber of benzoin OH

Table 3. DFT Predictions of Wavenumber Shifts^a and Intensity Changes for Pairs of S1, S2, and Benzoin

band	$\Delta\nu_1, \text{cm}^{-1}$	$R \equiv I/I_0$
System 1, (S2) NH \leftrightarrow O=C (S2)		
NH _s	-113	12.5
C=O _s	-26	2.00
NH _b	13	1.30
NH _b ^b	-34	4.67
C=O _b	-17	1.71
NH _b ^b	3	1.57
System 2, (S2) NH \leftrightarrow O (S2)		
NH _s	-80	8.10
NH _b	1	1.03
System 3, (B) OH \leftrightarrow O=C (B ^d)		
OH _s	-183	14.7
C=O _s	-32	1.4
System 4, (S1) C=O \leftrightarrow HO (B)		
(S1) C=O _s	-34	1.46
(B) OH _s	-192	13.1
System 5, (S2) C=O \leftrightarrow HO (B)		
(S2) C=O _s	-33	1.52
(B) OH _s	-208	16.7
System 6, (S1) NH \leftrightarrow O=C (B)		
(S1) NH _s	-107	9.20
(S1) NH _b	30	0.84
(B) C=O _s	-16	1.42
System 7, (S2) NH \leftrightarrow O=C (B)		
(S2) NH _s	-90	12.6
(S2) NH _b	22	0.70
(B) C=O _s	-14	1.71
System 8, (S1) NH \leftrightarrow OH (B)		
(S1) NH _s	-81	6.49
(S1) NH _b	29	0.91
(B) OH _s	-65 ^c	5.05
System 9, (S2) NH \leftrightarrow OH (B)		
(S2) NH _s	-90	9.32
(S2) NH _b	12	0.73
(B) OH _s	-18	0.84

^aWavenumber shifts $\Delta\nu$ are expressed as differences, while intensity changes are expressed as ratios. ^bNH \leftrightarrow O=C was fixed at 2.5 \AA .

^cFrequencies were affected by the phenyl group of the S1 side-chain model. ^dTwo H-bonds are formed between the two molecules.

groups in the gas phase (or in a nonpolar liquid phase such as carbon tetrachloride), where it is in the cis intramolecularly H-bonded conformation, is 3474 cm^{-1} .²⁹ No data are available for non-H-bonded trans-benzoin, because the preferred state is the H-bonded cis state, with $\Delta H = -14.76\text{ kJ/mol}$. Nonetheless, DFT calculations of non-H-bonded trans-benzoin predict a shift of ca. -167 cm^{-1} when the non-H-bonded trans-benzoin is converted to a cis intra-H-bonded state. Hence, the predicted wavenumber of the non-physically-existing non-H-bonded trans-benzoin OH stretch should be around 3650 cm^{-1} . The benzoin in the actual experimental solid state has much lower wavenumbers,

ca. 3415 and 3378 cm^{-1} (Figure 3). All results indicate that this benzoin must be in the trans conformation with strong intermolecular H-bonds, as suggested previously.²⁹ This inference has been confirmed further with single-crystal XRD results,³⁰ which show two populations of H-bonded trans molecules with two different orientations in the elementary cell. (See section 3.2.2 for a detailed spectral analysis.)

3.2.2. Detailed Spectral Analysis and DFT Calculations. Spectral deconvolution of NH stretching and C=O stretching bands reveals more accurately their wavenumbers and relative intensities (or peak areas) (Figure 4). The NH band for peak 2 shows a shift of ca. -40 cm^{-1} from peak 1, and the NH band for peak 3 shows a shift of ca. -137 cm^{-1} from peak 1 (Figure 4, top). The relative area intensities are 2%, 20%, and 78%, respectively. The intensity ratios of peaks 2 and 3 versus peak 1 are 10 and 39, respectively. The C=O peaks show shifts of -29 and -48 cm^{-1} (Figure 4, bottom). The relative area intensities are 19%, 74%, and 7%, respectively.

To further interpret these results quantitatively in terms of relative group populations, DFT simulations were done for NH groups of S2 chains interacting with C=O groups of S2 chains, to describe the most probable interchain H-bonds in the polymer. The results (system 1, Table 3) show a wavenumber shift of -113 cm^{-1} and a large intensity enhancement by a factor of 12.5. Hence, the relative areas observed in Figure 4 do not represent the relative group populations. It appears that peak 3, which has a shift of -137 cm^{-1} , represents NH groups strongly bonded to C=O groups. If we use the intensity ratio R of 12.5 for peaks 1 and 3, then the relative population for the groups of peak 3 is $78/12.5 \approx 6$, or 3 times larger than the population for peak 1. The predicted energy of this H-bond is quite high, -23.03 kJ/mol ; see system 1 in Table A in Supporting Information. The predicted H-bond length d and angle θ are 1.98 \AA and 169° , indicating a strong H-bond. NH peak 2 with $\Delta\nu = -40\text{ cm}^{-1}$ represents either NH groups H-bonded with medium-strength H-bonds to C=O groups, or NH groups bonded to O atoms in the backbone or side chains or to both. For the former case, a simulation with Δd fixed at 0.25 nm predicts an energy of -17.35 kJ/mol , a wavenumber shift of $\Delta\nu = -33\text{ cm}^{-1}$ (scaled as ca. $40 \times 113/137$), and an intensity enhancement $R = 4.67$. Then the relative population of peak 2 is predicted to be $20/4.67 = 4.3$. Therefore, this approach predicts relative populations of 2:4.3:6, or about 1:2:3, for the three groups. A lower energy of the H-bond (S2) NH \leftrightarrow O (S2) was obtained from the DFT simulations (see system 3 in Table A, Supporting Information). DFT calculations for the H-bond (S2) NH \leftrightarrow O (backbone) (see system 4 in Table A, Supporting Information) predict that it has a similar binding strength as (S2) C=O \leftrightarrow HN (S2). Upon H-bonding, the NH-bending band is predicted to have a positive wavenumber shift of 13 cm^{-1} . The predicted intensity enhancement is small, about 1.3. This band is not as sensitive as the NH stretching band for probing the relative populations of the NH groups.

Simulations of the H-bonding between NH and C=O groups provide a wavenumber shift of -26 cm^{-1} for the C=O groups. This value is close to the observed value of -29 cm^{-1} for peak 2. If peak 2 corresponds to this H-bonded population, the predicted intensity ratio is 2, and the relative population of the C=O groups for peak 2 versus those for peak 1 is 2:1. It is unclear what is the origin of peak 3, which represents a quite small relative population. Its wavenumber shift of -52 cm^{-1} is quite large, making it unlikely that the predicted value represents peak 2.

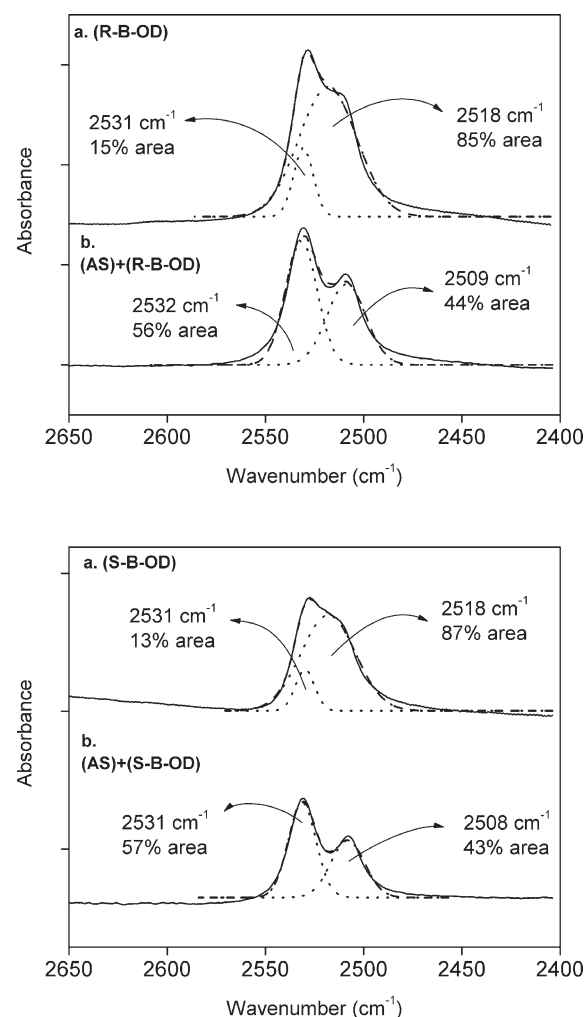


Figure 5. ATR-IR spectra of the OD stretching bands of (R)- and (S)-benzoin alone and with AS. (Top panel) (a) R-B-OD and (b) AS + R-B-OD; (bottom panel) (a) S-B-OD and (b) AS + S-B-OD. The fits to the deconvolution spectra are good: $R^2 = 0.993, 0.988, 0.997$, and 0.990 from top to bottom. Results for relative areas of the two enantiomers are the same within experimental error of 2%.

No DFT predictions of such a high value are available. These results will be discussed further after the MD simulations, which include a large diversity of H-bonded states and which will be used in docking studies of AS with B. Nonetheless, the results are consistent with the NH stretch results. Probably, about $5/6 \approx 80\%$ of the NH groups form H-bonds with C=O groups of the side chains and with some O groups of the backbone.

Since the OH band of benzoin overlaps with the NH band of AS, deuterated benzoin-OD was used to shift the hydroxyl band and help distinguish the two bands. The OH bands at 3415 and 3378 cm^{-1} shift to 2531 and 2518 cm^{-1} upon deuterium substitution for both enantiomers (Figure 5). These wavenumbers compare well to the values of 2532 and 2507 cm^{-1} reported by Pawelka et al.,²⁹ who used benzoin-OD of higher purity of ca. 70%. The shifts occur because the reduced mass of OH is about 90% larger than the reduced mass of OD. The relative areas for each enantiomer are the same, $15\% \pm 2\%$ for the medium H-bonded and $85\% \pm 2\%$ for the strongly H-bonded OD groups. Upon absorption of B by AS, the OD band changes significantly,

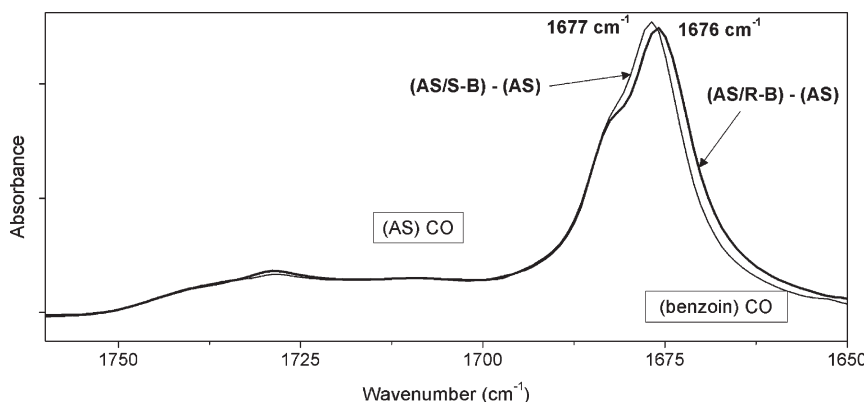


Figure 6. Difference spectra of the CO stretching bands of absorbed benzoin and of AS polymer upon interacting with (*R*)-benzoin (thick line) and (*S*)-benzoin (thin line). The effect on the polymer bands is the same for both enantiomers. The effect of AS on the benzoin band is small but significant; see text for details.

and the NH band changes little. This suggests that there is no H–D exchange for the AS polymer. Since the 2518 cm^{-1} peak disappears, we infer that there is no pure solid benzoin left in the area examined by ATR (at the penetration length of about $1\text{ }\mu\text{m}$ above the ATR plate). Hence, all benzoin observed is absorbed by the AS sample and has a different spectral “signature”. The absorbed benzoin is also present in two populations. One population is medium H-bonded at $2531 \pm 1\text{ cm}^{-1}$, the same as for pure solid benzoin, probably by coincidence. The other one, at 2508 cm^{-1} , corresponds to an even more strongly H-bonded state than in pure benzoin. Moreover, upon benzoin absorption the relative areas of the two peaks change to $56\% \pm 1\%$ and $44\% \pm 1\%$, indicating again the different state of H-bonding between benzoin and AS versus pure benzoin. The (*R*)- and (*S*)-benzoin enantiomers interact similarly and strongly with AS.

This result is quite significant. Both enantiomers form an equally strong H-bond with the polymer. This implies that the additional interaction of (*R*)-benzoin inferred from the retention factors (see section 3.1) is not due to a stronger H-bond but to an additional bond, which is more probably an H-bond than a $\pi-\pi$ interaction.

DFT simulations were done to predict the following: (a) wavenumbers and intensities of various key bands of S1 and S2 chains and of benzoin (Table 2); (b) shifts in wavenumbers and intensity changes of the bands after H-bonding interactions (Table 3); and (c) energies, lengths, and angles of these H-bonds (Table A in Supporting Information). Several of these H-bonding interactions will now be described in detail, and the results will be summarized at the end of this section.

The simulations of OH of *trans*-benzoin H-bonded to C=O of benzoin predict a high wavenumber shift (-183 cm^{-1} system 3 in Table 3), and a huge intensity ratio $R = 14.7$. For C=O, the respective values are -32 cm^{-1} and 1.4. When one benzoin molecule forms two H-bonds with another benzoin molecule, the energy difference per H-bond is -23.78 kJ/mol (see system 6 in Table A, Supporting Information). This energy difference is quite a bit higher than the predicted energy difference (-14.76 kJ/mol) of an intramolecular H-bond of *cis*-benzoin (Table A, Supporting Information). The H-bond energy of a (B) OH group with an (S1) C=O group is much larger (-33.31 kJ/mol) than the H-bond between (B) OH and (B) B C=O. The predicted wavenumber shift is only slightly higher in absolute value, -192 versus -183 cm^{-1} . The fair predictions of wavenumber shifts

provide some confidence in the accuracy of the predictions of H-bond energies, which are not directly measurable.

The interactions of single AS chains, model chain S1 (which has a benzene ring) and model chain S2 (which has no benzene ring), with benzoin were also simulated with DFT. When either chain hydrogen-bonds to benzoin, its C=O wavenumber shifts by 34 cm^{-1} . This shift is higher than the shift of 26 cm^{-1} of the C=O group of AS bonded to the NH group of AS. The intensity enhancement (1.46 or 1.52) is smaller. The respective shift in the wavenumber of benzoin OH groups with S2 is -192 cm^{-1} , which is larger by 5% than the value of -183 cm^{-1} for B–B. This relative shift is exactly what was observed for the second OH peak (Figure 5). These results suggest that when benzoin enters the polymer cavities, the H-bonds between B and B break and stronger bonds form between the groups (B) OH [or (B) OD] and C=O of the polymer. Indeed, the predicted energy of this S1–B H-bond is -35.03 kJ/mol , which is larger (in absolute value) than the value of -23.78 kcal/mol between B and B. For the simpler chain S1, the predicted H-bond energy is also large, -33.31 kcal/mol .

When the NH groups of S1 or S2 interact with the C=O groups of benzoin, the NH stretch wavenumber shifts by -107 cm^{-1} for S1 and by -90 cm^{-1} for S2 ($R = 9.20$; Table 3). This number differs by only 20% from the value of -113 cm^{-1} predicted by DFT for the S2–S2 interaction (system 1, Table 3). The energies are also comparable, at -23.03 kJ/mol for S2 with S2 versus -18.39 kJ/mol for S2 with B and -24.20 kJ/mol for S1 with B. (The value for the energy of S1 with S1 is not available, because the computations would take too much time.) Predictions of $\Delta\nu$ for NH-bending are $+30$ and $+22\text{ cm}^{-1}$, which are higher than the value of 13 cm^{-1} between S2 and S2. The C=O stretch band shifts by -34 cm^{-1} for S1 or -33 cm^{-1} for S2 with B, versus -26 cm^{-1} for S2 with S2. Overall, the DFT predictions are fairly accurate.

The interactions between NH groups of AS and OH groups of benzoin are predicted to be weaker than those between C=O groups of AS and OH groups of benzoin. The H-bond energies are -16.55 or -12.25 kJ/mol for the S1 or S2 chain, respectively. The wavenumber shifts are also smaller, -81 or -90 cm^{-1} , respectively.

In summary, on the basis of DFT predictions and IR results, the following inferences are made:

- (1) In the pure polymer, most of the NH groups tend to form hydrogen bonds primarily with the C=O groups. At least

Table 4. Hydrogen-Bonding Conditions of NH and CO Groups of the Central Unit Cell (5–8-mer) for AS Model^a

side chain	H-bond with	length (Å)	SD	angle (deg)	SD
(a) H-Binding Status of NH Groups					
5-mer C2	5-mer C3 CO	2.89	0.12	140	4.62
5-mer C3	6-mer C2 O	3.84	0.13	100	5.06
5-mer C5	6-mer O6	3.52	0.09	130	7.68
6-mer C2	6-mer C3 CO	2.37	0.08	135	4.21
6-mer C3	7-mer C2 O	2.86	0.08	160	5.70
6-mer C5	7-mer O6	3.46	0.06	142	5.30
7-mer C2	7-mer C3 O	2.78	0.11	132	4.39
7-mer C3 ^b					
7-mer	8-mer O6	3.25	0.07	152	5.49
8-mer C2 ^b					
8-mer C3	10-mer C5 O	3.63	0.21	146	13.48
8-mer C5	9-mer O6	2.89	0.07	148	5.83
(b) H-Binding Status of CO Groups					
5-mer C2 ^b					
5-mer C3	5-mer C2 NH	2.89	0.12	140	4.62
5-mer C5	3-mer C3 NH	3.90	0.12	145	4.79
6-mer C2 ^b					
6-mer C3	6-mer C2 NH	2.37	0.08	135	4.21
6-mer C5	4-mer C3 NH	3.67	0.12	129	4.92
7-mer C2 ^b					
7-mer C3	7-mer C2 NH	2.78	0.11	132	4.39
7-mer C5 ^b					
8-mer C2 ^b					
8-mer C3 ^b					
8-mer C5 ^b					

^a Forty frames were randomly chosen for averaging; see Figure 7. ^b Not available.

three populations were identified by the relative strength of the H-bonds. The relative populations for NH are 1:2:3. NH may also form H-bonds with certain O atoms on the polymer backbone. At least three populations of C=O groups were identified.

- (2) Pure solid benzoin is in the trans conformation. All OH groups are intermolecularly H-bonded with C=O groups, in two populations, (i) strong H-bonds and (ii) very strong H-bonds.
- (3) When benzoin is absorbed by AS, these H-bonds break, and benzoin OH (or OD) groups form two different kinds of H-bonds with C=O of AS, corresponding to two populations. One population is H-bonded with the same strength as B–B. The groups of the other population are bonded more strongly than the groups with the strongest bonds between B and B.
- (4) When (R)- or (S)-benzoin molecules are absorbed by AS, their C=O groups may form H-bonds with the NH groups if it is sterically allowed. These H-bonds have

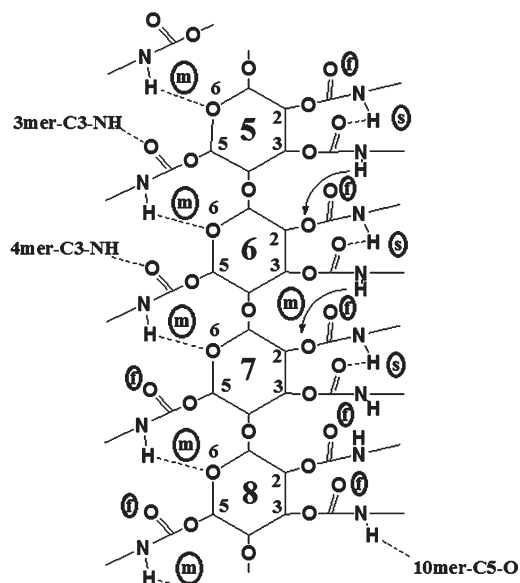


Figure 7. Two-dimensional representation of possible binding sites, NH, CO, and O, of a 12-mer AS polymer model in the central units (monomers 5–8), as predicted from MD simulations. s = strong H-bond; m = medium-strength H-bond; f = free (or weakly bonded) group; see text and Table 4.

Table 5. Structural Information and Specific Binding Sites of AS with (R)- and (S)-Benzoin for Cavity A from MD Simulations^a

	cavity A
no. of side chains and accessible functional groups	4-mer C3 Ph
(R)-benzoin OH	6-mer C5 Ph
(R)-benzoin CO	7-mer C5 Ph and CO
(R)-benzoin Ph	8-mer C2 Ph, CO, and NH
(S)-benzoin OH	8-mer C2 CO ($1.80 \pm 0.09 \text{ \AA}$; $162^\circ \pm 7.34^\circ$)
(S)-benzoin CO	8-mer C2 NH ($2.57 \pm 0.17 \text{ \AA}$; $143^\circ \pm 8.94^\circ$)
(S)-benzoin Ph	6-mer C5 Ph, T-shape; 7-mer C5 Ph, parallel
$\Delta E_R - \Delta E_S$	7-mer C5 CO ($3.14 \pm 0.14 \text{ \AA}$; $65^\circ \pm 7.62^\circ$)
^a Shown in parentheses are the H-bond lengths and angles. ^b Not available.	b 4-mer C3 Ph, T-shape
	$-56 \pm 19 \text{ kJ/mol}$

slightly lower energies than those between NH (AS) and C=O (AS).

An important question is whether these IR results can be used to detect, directly or indirectly, any enantioselective interactions between AS and B. Taking the difference between spectra

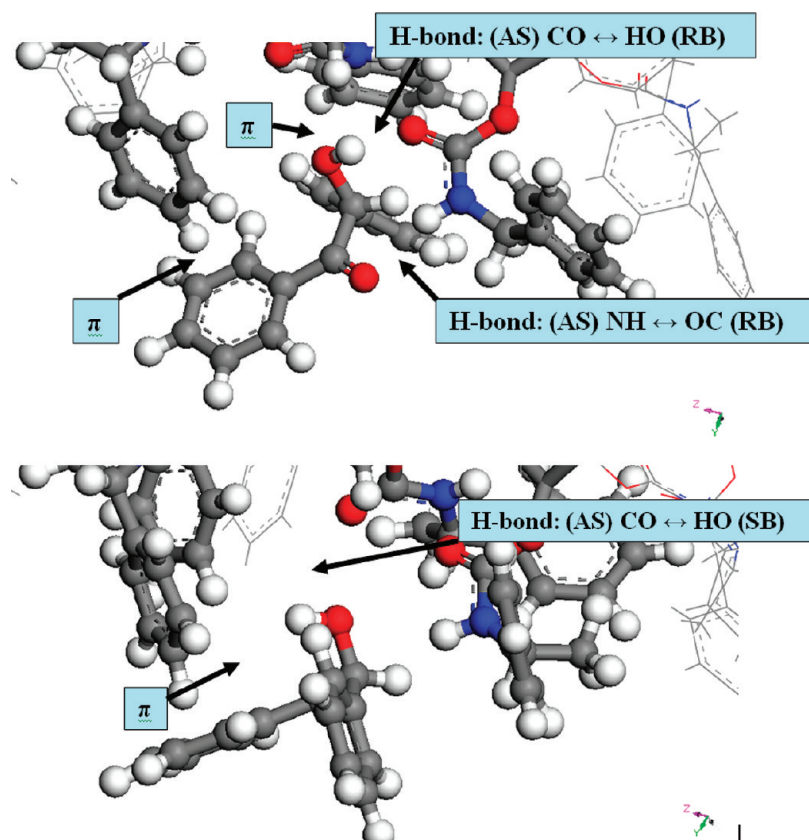


Figure 8. MD simulation predictions of docking of (R)-benzoin (top) and (S)-benzoin (bottom) in cavity A. This simulation predicts four significant interactions (two H-bonds and two $\pi-\pi$ interactions) for R-B and two interactions (one H-bond and one $\pi-\pi$ interaction) for S-B. This simulation predicts enantioselectivity for this cavity.

(AS + R-B) – AS and (AS + S-B) – AS in the 1760–1640 cm^{-1} region, we observe the following in the difference spectra (Figure 6):

- (A) Between 1760 and 1700 cm^{-1} , where the C=O bands of AS are expected, the absorbance differences are exactly the same for both enantiomers. This implies that the H-bonded state of the AS C=O groups changes upon absorption of benzoin and that the changes are the same when either enantiomer is absorbed.
- (B) Between 1700 and 1640 cm^{-1} , where the C=O band of benzoin is expected to appear, there is a small and reproducible wavenumber difference of ca. 1 cm^{-1} . This difference is higher than the estimated error of $\pm 0.2 \text{ cm}^{-1}$. This result suggests that (S)-benzoin interacts less strongly with AS than (R)-benzoin. This inference is novel and is supported by MD results.

3.3. Molecular Mechanics/Molecular Dynamics/Monte Carlo Results. 3.3.1. Overview of Models Used. Although the DFT calculations are presumed to lead to fairly accurate predictions of electrostatic interactions and H-bonding interactions, they are limited to small-scale systems. In order to understand the enantiomeric interactions involving polymers with chiral cavities, we had to use molecular simulations for structural predictions and for docking studies in an effort to understand plausibly the molecular basis for the observed enantioselectivity.

A 12-mer AS polymer with a 4-fold helix and three unit cells was built as the simplest model (see section 2.4.2). This model is similar to the one used by Kasat et al.⁷ but smaller than the 36-mer used for AD by Li et al.¹⁹ Only monomers 5–8 at the center

were examined for their possible cavities and the docking studies, to avoid possible end effects.

The CVFF force field was chosen for most of these simulations. The accuracy of this force field was evaluated, by comparison to DFT predictions of five types of H-bonds and one $\pi-\pi$ interaction (Table B in Supporting Information). The percent differences vary from 7% to 130% for energies, from 1% to 10% for distance, and from 1% to 7% for angles. Hence, the predictions should be considered as semiquantitative. These differences were significantly smaller than those determined with four other force fields available in Material Studio (PCFF, COMPASS, Dreiding, and Universal). Kasat et al.⁷ used the CVFF and PCFF force fields. Li et al.¹⁹ used the COMPASS force field. The accuracy of the IR predictions based on these force fields is generally rather poor, probably because only classical mechanical effects are considered.

3.3.2. MD Simulations of Pure AS Polymer. The helical pitch of the AS backbone was fixed at 1.46 nm, as inferred from the XRD results. The predicted diameter of the AS rod was ca. 1.70 nm, which fits well the XRD result of 1.69 nm.⁷ The agreement gives some additional confidence in the MD predictions.

Detailed binding states of the NH and C=O groups of AS as predicted are shown in Table 4. The data were averaged by randomly choosing 40 frames from the equilibrium states. The 2D representation of the AS binding structure is shown in Figure 7, as a 2D projection of the 3D representation. This representation allows us to point out the H-bonds more clearly than by showing images of the 3D structures. In this figure, we can identify three

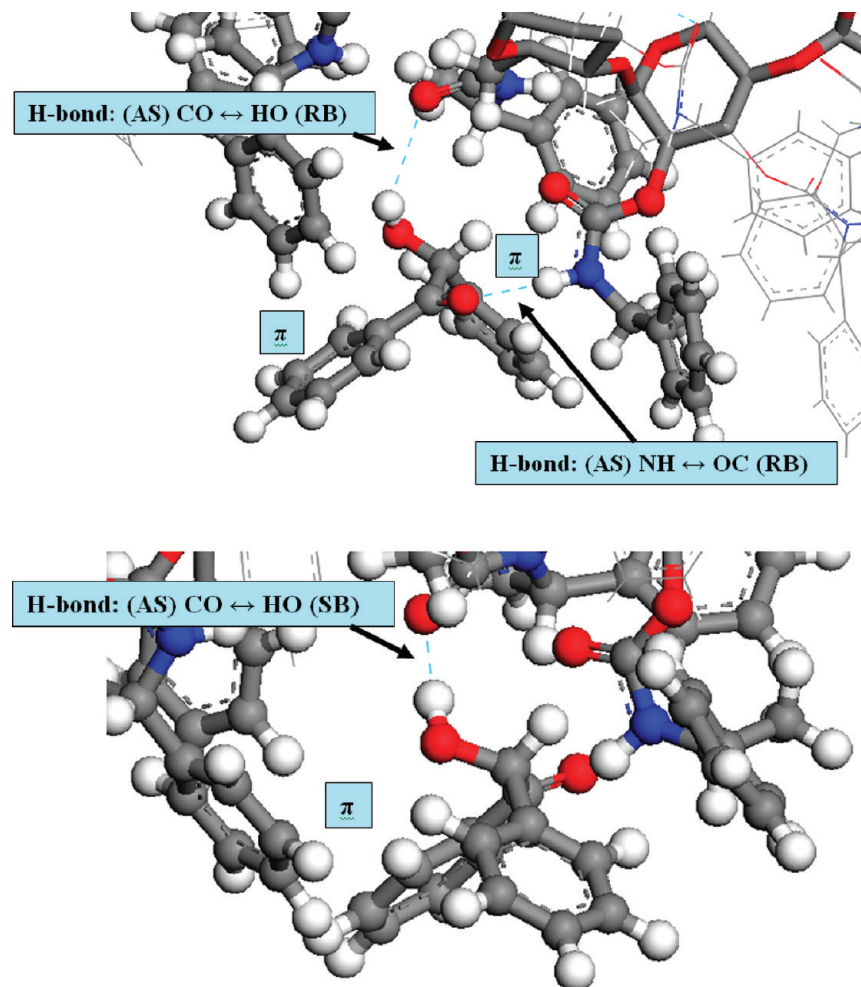


Figure 9. MC simulation predictions of docking of (*R*)- and (*S*)-benzoin in cavity A. This simulation predicts four interactions, (two H-bonds and two $\pi-\pi$ interactions) for R-B and two interactions (one H-bond and one $\pi-\pi$ interaction) for S-B. This simulation predicts enantioselectivity for this cavity.

types of NH groups, which have either a strong (s) bond with C=O groups (type i) or a medium (m) strength bond with O atoms (type ii) or a weak bond or “free” (f) (type iii), as judged from the bond distances and angles. The relative populations of these groups in this MD model are 4:5:3 (f:m:s). The percentage of “free” NH groups (about 30%) is slightly larger than the results (1:2:3 or about 17%) inferred from IR of the actual polymer and DFT. This suggests that there may be some additional H-bonds between adjacent molecules in the actual polymer material. More specifically, the type I bonds seem to occur between the C2 side chains of monomers 5–8 bonding with C=O groups of the C3 side chain. Type ii bonds seem to occur between the C5 side chains of monomer 5 (or 6, or 7) bonding with O atoms of monomer 6 (or 7, or 8, respectively).

The simulation results in Table 4 suggest that some NH groups of AS tend to form intrapolymer H-bonds, leaving fewer NH groups available to bind with benzoin (or other solutes). The OH groups of benzoin are more likely to bind with C=O and NH groups of AS, whereas the C=O groups of benzoin can only bind with the NH groups of AS, as shown in the docking simulations below.

3.3.3. MD and MC Docking Simulation Studies of Benzoin Enantiomers in AS Polymer.

MD docking simulation results are

summarized in Table 5 and Figure 8. Cavity A, which is the largest cavity among those observed, was chosen for these MD simulations. The results show that (*R*)-benzoin could form two H-bonds simultaneously with the same side chain, the C2 chain of the eighth monomer, whereas (*S*)-benzoin could only form the H-bond (SB) OH \leftrightarrow O=C (AS). The predicted energy difference indicated that (*R*)-benzoin interacts more strongly with AS than (*S*)-benzoin by -56 ± 19 kJ/mol. The results appear to match the inferences from the IR spectral analysis. Since the MD docking simulation predictions can depend on the chosen initial orientation of the benzoin molecule in the cavity, as inferred from the IR results, the MD results could be biased and may have less predictive value.

The MC docking simulation results are given in Figures 9 and 10 and Table 6. Cavities A and B could be identified as having sufficient size and accessible binding sites for R-B and S-B. Inside cavity A, there is one NH group and two C=O groups that are exposed and free. The simulations showed that R-B could form two H-bonds, (AS) C=O \leftrightarrow HO (RB) and (AS) NH \leftrightarrow OC (R-B), and two $\pi-\pi$ interactions, whereas S-B could form one H-bond, (AS) C=O \leftrightarrow HO (S-B), and one $\pi-\pi$ interaction. The complex docking configurations predicted by MC are different from those predicted by the MD simulations. The reason S-B could

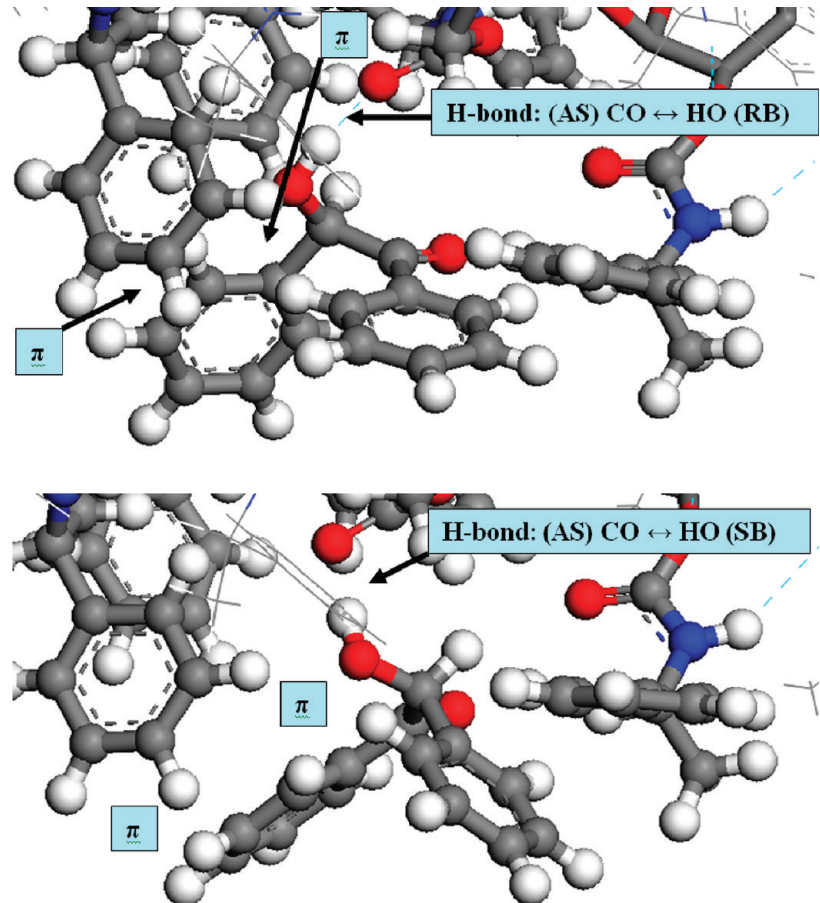


Figure 10. MC simulation predictions of docking of (*R*)- and (*S*)-benzoin in cavity B. This simulation predicts three interactions (one H-bond and two $\pi-\pi$ interactions) for R-B and three interactions (one H-bond and two $\pi-\pi$ interactions) for S-B. This simulation predicts no enantioselectivity for this cavity.

Table 6. Structural Information and Most Important Specific Binding Sites with (*R*)- and (*S*)-Benzoin for Cavities A and B from MC Simulations^a

	cavity A	cavity B
no. of side chains and accessible functional groups	4-mer C3 Ph 6-mer C5 Ph 7-mer C5 Ph and CO 8-mer C2 Ph, CO, and NH	3-mer C3 Ph 4-mer C2 Ph 6-mer C5 Ph and CO 7-mer C2 Ph and CO
(<i>R</i>)-benzoin OH	7-mer C5 CO (2.85 Å; 132°)	6-mer C5 CO (1.68 Å; 171°)
(<i>R</i>)-benzoin CO	8-mer C2 NH (2.15 Å; 158°)	<i>b</i>
(<i>R</i>)-benzoin Ph	6-mer C5 Ph, T-shape; 7-mer C5 Ph, T-shape	6-mer C5 Ph, T-shape; 7-mer C2 Ph, T-shape
(<i>S</i>)-benzoin OH	7-mer C5 CO (1.66 Å; 156°)	6-mer C5 CO (1.71 Å; 176°)
(<i>S</i>)-benzoin CO	N/A	N/A
(<i>S</i>)-benzoin Ph	4-mer C3 Ph, T-shape	6-mer C5 Ph, T-shape; 7-mer C2 Ph, T-shape
$\Delta E_R - \Delta E_S$	+48 kJ/mol	-0.9 kJ/mol

^a Shown in parentheses are the H-bond lengths and angles. ^b Not available.

not bind with the NH group of the cavity is as follows. As the OH group of S-B binds with the AS C=O group, its C=O group finds itself at an unfavorable orientation for binding with the NH group. In addition, the large steric hindrance effect caused by its

two phenyl groups does not allow the rotation needed to obtain a favorable orientation. Evidently, the different R-B configuration allows it to form the second H-bond. Hence, cavity A allows a substantial enantioselectivity. Cavity B has two C=O groups for

Table 7. Structural Information and Most Important Specific Binding Sites with (R)- and (S)-Benzoin for Cavities A and B from MD Simulations^a

	cavity A	cavity B
no. of side chains and accessible functional groups	4-mer C3 Ph 6-mer C5 Ph 7-mer C5 Ph and CO 8-mer C2 Ph, CO, and NH	3-mer C3 Ph 4-mer C2 Ph 6-mer C5 Ph and CO 7-mer C2 Ph and CO
(R)-benzoin OH	7-mer C5 CO ($3.41 \pm 0.27 \text{ \AA}$; $125^\circ \pm 6.44^\circ$)	6-mer C5 CO ($1.89 \pm 0.10 \text{ \AA}$; $123^\circ \pm 4.86^\circ$)
(R)-benzoin CO	8-mer C2 NH ($2.06 \pm 0.07 \text{ \AA}$; $168 \pm 7.25^\circ$)	<i>b</i>
(R)-benzoin Ph	6-mer C5 Ph, T-shape; 7-mer C5 Ph, parallel	3-mer C3 Ph, T-shape; 3-mer C3 Ph, T-shape
(S)-benzoin OH	7-mer C5 CO ($3.28 \pm 0.10 \text{ \AA}$; $136 \pm 5.85^\circ$)	6-mer C5 CO ($2.13 \pm 0.12 \text{ \AA}$; $149 \pm 8.54^\circ$)
(S)-benzoin CO ^b	4-mer C3 Ph, T-shape	3-mer C3 Ph, T-shape
$\Delta E_R - \Delta E_S$	$-62 \pm 20 \text{ kJ/mol}$	$-26 \pm 24 \text{ kJ/mol}$

^a Initial orientations and configurations are from the results of MC simulations. Shown in parentheses are the H-bond lengths and angles. ^b Not available.

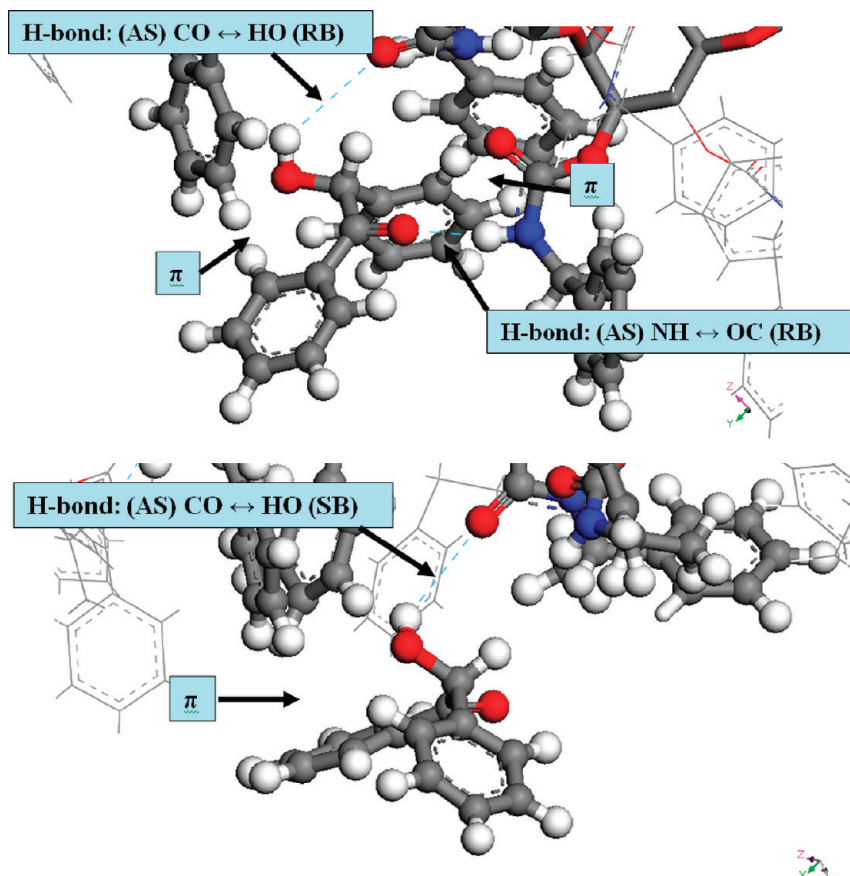


Figure 11. MC/MD simulation predictions of docking of (R)- and (S)-benzoin in cavity A. The initial orientations and configurations are from the results of MC simulations. This simulation predicts four interactions (two H-bonds and two $\pi-\pi$ interactions) for R-B and two interactions (one H-bond and one $\pi-\pi$ interaction) for S-B. This simulation predicts enantioselectivity for this cavity.

possible H-bonding sites with OH groups. The simulation results indicate that, for cavity B, both R-B and S-B enantiomers have the same binding configuration, one H-bond, (AS) $\text{C}=\text{O} \leftrightarrow \text{HO}$ (B), and two $\pi-\pi$ interactions. Hence, no pronounced enantioselectivity is predicted for this cavity. The binding in cavity

B may tend to decrease the predicted overall (or average) enantioselectivity, compared to the enantioselectivity in cavity A alone.

The energies in Table 6 show that although (R)-benzoin could form two H-bonds in cavity A, its energy is higher than that of

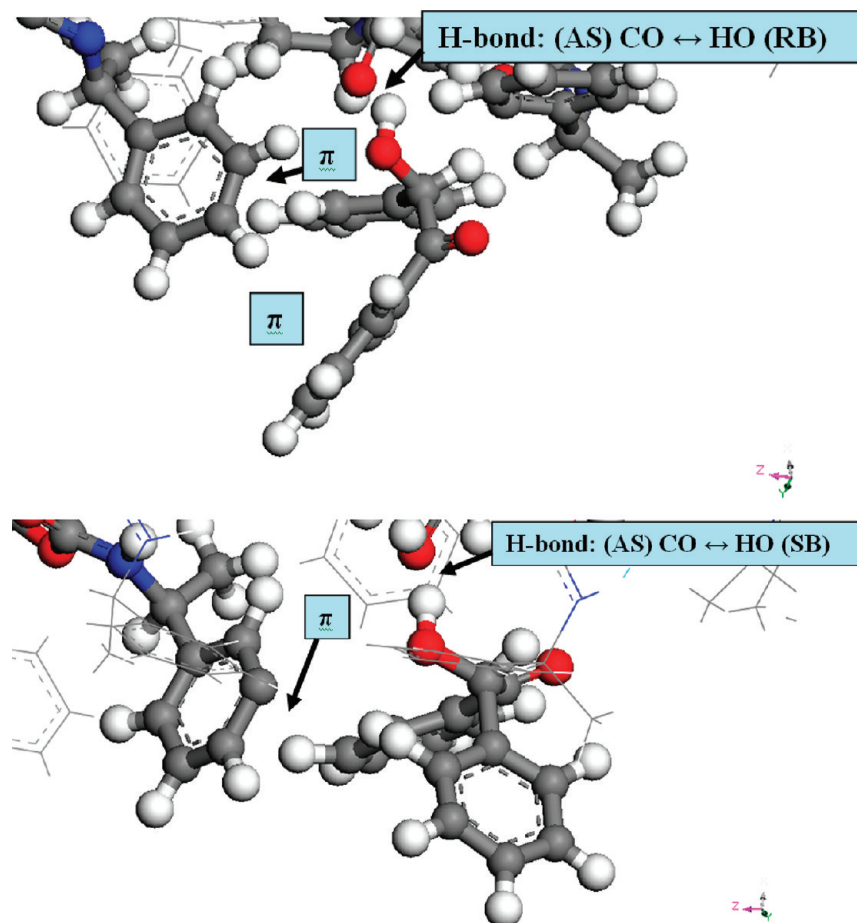


Figure 12. MC/MD simulation predictions of docking of (*R*)- and (*S*)-benzoin in cavity B. Initial orientations and configurations are from the results of MC simulations. This simulation predicts three interactions (one H-bond and two $\pi-\pi$ interactions) for R-B and two interactions (one H-bond and one $\pi-\pi$ interaction) for S-B. This simulation predicts no enantioselectivity for this cavity.

(*S*)-benzoin by +48 kJ/mol. The reason leading to the reverse enantioselectivity in energies is probably the unrealistic predicted value of the H-bond length, which is $d = 1.66 \text{ \AA}$, of the (AS) C=O \leftrightarrow HO (B) type of H-bond, as shown in Table B in Supporting Information. The energies for this H-bond formed by (*S*)-benzoin with AS are overestimated.

To improve the MC simulation predictions and produce more accurate energy predictions with more realistic H-bond distances, the results from the MC simulations were used as the initial orientations and configurations for the subsequent MD simulations. The results are shown in Figures 11 and 12 and Table 7. Since the atoms were allowed to move from the positions predicted from MC simulations, more plausible H-bond lengths were predicted, $d = 3.41 \pm 0.27 \text{ \AA}$. The bonding configurations remained the same, however, as in the MC simulations. The energy difference, $\Delta E = -62 \pm 20 \text{ kJ/mol}$, would lead to a predicted enantioselectivity value of $S \approx 7 \times 10^{10}$ for benzoin in cavity A and $\Delta E \approx \Delta G$ if all interactions involved cavity A. Cavity B also showed a small energy enantioselectivity of $\Delta E = -26 \pm 24 \text{ kJ/mol}$, in which the average value is close to the standard deviation. Hence, this cavity could be regarded as being nearly nonenantioselective.

In summary, the MC/MD docking simulations seem to be suitable for predicting or explaining some of the HPLC/IR data presented here. They suggest that there are two possible

docking cavities that could have strong interactions with the benzoin molecule. Cavity A is quite enantioselective, and cavity B is nearly nonenantioselective. In all potential binding configurations, both the R-B and S-B enantiomers could form the (AS) C=O \leftrightarrow HO (B) type of H-bond, which is also the strongest H-bond, as inferred from DFT calculations. The AS structure described in Table 4 suggests that there are more accessible C=O groups than NH groups. The H-bond type (AS) C=O \leftrightarrow HO (B) may be the easiest bond to form. The key enantioselective interaction would involve another H-bond, (AS) NH \leftrightarrow OC (RB), which may form simultaneously by R-B in cavity A. The MC and MC/MD results are consistent with the IR, HPLC, and DFT results. (*R*)-Benzoin interacts more strongly and tends to form two H-bonds simultaneously with AS. The MC results lead to the predictions that OH groups of both (*R*)- and (*S*)-benzoin bind similarly with the C=O groups of AS, as inferred from IR data. The key chiral distinction arises from the binding, or nonbinding, of the NH group. This binding is controlled to some extent by the steric effects of the phenyl rings. The $\pi-\pi$ interactions are also somewhat different for the two enantiomers. Hence, the MC/MD method seems to be more suitable for elucidating realistically, and perhaps predicting, the basis for the observed enantioselectivity of benzoin and for testing hypotheses derived from HPLC, IR, and DFT simulations.

4. CONCLUSIONS

HPLC results show that retention factors of benzoin enantiomers with the sorbent AS increase with decreasing concentration of IPA in the IPA/hexane mobile solvent phase, as expected since the solvent becomes more hydrophobic. The retention factors are higher for (*R*)-benzoin. For pure *n*-hexane, the retention factors are the highest and the enantioselectivity $S \equiv k_R/k_S$ is the highest, 2.13, compared to a range of 1.79–1.44 for IPA/hexane from 10 to 0.5 vol % IPA. Detailed IR spectroscopic results and DFT simulations provide unique novel information on the state of hydrogen bonding of the NH and C=O groups in pure AS. There are three populations of NH groups, as classified from the strength of their hydrogen bonding: weakly or non-H-bonded, medium H-bonded, and strongly H-bonded. DFT simulations reveal that, upon H-bonding, the NH stretch band shifts by up to 113 cm^{-1} and the band intensity increases by up to 12.5-fold. On the basis of these results, the relative populations are 1:2:3 or ca. 17%–33%–50%, even though the relative areas are 2%–20%–78%. Similarly, there are three populations of H-bonded C=O groups. The NH groups bind mostly with C=O groups in the surrounding side chains and partly with the O-groups in the backbone.

The structure of the polymer cavities is determined with MD simulations, for monomers 5–8 of a 12-mer polymer model. These simulations are done with the CVFF force field, which seems to be more accurate than several other force fields tested in Materials Studio, as found by comparison to DFT simulations. Such MD simulations are still rather inaccurate but they provide a comprehensive picture of the polymer structure, including the existence of chiral cavities capable of accommodating one benzoin molecule.

Enantioselective interactions of AS with benzoin enantiomers are studied via IR data and DFT simulations. By using pure *n*-hexane as the mobile phase, the key interactions of our system can be plausibly predicted with a two-component model system of sorbent and benzoin. DFT simulations are used for estimating H-bonding strengths. It is inferred that, without steric hindrance, benzoin may tend to form the type of H-bond (AS) C=O \leftrightarrow HO (B), which is the strongest H-bond for the side chain/B pairs. H–D exchange allowed direct observation of the OH bands of benzoin. Both enantiomers form identical H-bonds with AS. Moreover, difference spectra suggest that the C=O groups of (*R*)-benzoin bind differently with AS than those of (*S*)-benzoin. These bonds are inferred to be the key difference for the mechanism of chiral recognition of B by AS.

Since, as suggested from the literature, the environment in the chiral cavities plays a key role in enantioselectivity, MD, MC, and hybrid MD/MC docking studies are used to model AS/B interactions. These molecular simulations suggest that, for some potentially enantioselective cavities, (*R*)-benzoin may form two H-bonds with AS simultaneously and have two significant $\pi-\pi$ interactions, whereas (*S*)-benzoin tends to form one type of H-bond, (SB) OH \leftrightarrow O=C (AS), and have one significant $\pi-\pi$ interaction. For some of those cavities, the differences in the numbers of H-bonds and $\pi-\pi$ interactions between AS and the two benzoin enantiomers appear to be the main reason for the predicted and observed enantioselectivity.

4.1. Some Additional Concluding Remarks. Future simulations of one- and two-component systems may shed more light on the effects of interpolymer interactions (involving two or more polymer rods). For three-component (sorbent–solute–solvent)

systems, the effect of *n*-hexane, which is expected to be minor, may be examined. For four-component systems, the effect of the polar solvent, IPA or other, may be quite strong, since such a solvent affects the polymer structure as well as the polymer–solute and solute–solvent interactions.^{6,15,18}

The overall enantioselectivity may depend not only on strong enantioselective interactions for the optimal cavities discovered here but also on less enantioselective interactions with other cavities and other sites between the polymer rods. Hence, MC/MD simulations such as those used here may not lead to quantitative predictions of relative energies and enantioselectivities.

■ ASSOCIATED CONTENT

Supporting Information. Two tables, containing detailed DFT simulation predictions of H-bond energies, lengths, and angles for pairs of S2 with S2, B with B, and S1 or S2 with B and comparisons of DFT predictions of H-bond parameters with MM simulation predictions. This material is available free of charge via the Internet at <http://pubs.acs.org>.

■ AUTHOR INFORMATION

Corresponding Author

*E-mail frances@purdue.edu; phone 765-494-4078; fax (765) 494-0805.

Present Addresses

[†]DuPont Company, 4417 Lancaster Pike, Wilmington, DE.

■ ACKNOWLEDGMENT

This research was supported by an NSF grant, CBET 0854247. We thank Dr. Geoffrey Cox from Chiral Technologies (West Chester, PA) for helpful advice and for supplying the ChiralPak AS silica beads and columns. We thank Dr. Srinivas Janaswamy (Department of Food Sciences, Purdue University) for help in generating the polymer helical structure.

■ REFERENCES

- (1) Okamoto, Y.; Yashima, E. *Angew. Chem., Int. Ed.* **1998**, *37*, 1020–1043.
- (2) Lammerhofer, M. *J. Chromatogr. A* **2010**, *1217*, 814–856.
- (3) Kasat, R. B.; Frances, E. I.; Wang, N.-H. L. *Chirality* **2010**, *22*, 565–579.
- (4) Kasat, R. B.; Wee, S. Y.; Loh, J. M.; Wang, N. H. L.; Frances, E. I. *J. Chromatogr. B* **2008**, *875*, 81–92.
- (5) Kasat, R. B.; Wang, N. H. L.; Frances, E. I. *Biomacromolecules* **2007**, *8*, 1676–1685.
- (6) Kasat, R. B.; Zvinevich, Y.; Hillhouse, H. W.; Thomson, K. T.; Wang, N. H. L.; Frances, E. I. *J. Phys. Chem. B* **2006**, *110*, 14114–14122.
- (7) Kasat, R. B.; Wang, N. H. L.; Frances, E. I. *J. Chromatogr. A* **2008**, No. 1190, 110–119.
- (8) Wirz, R.; Burgi, T.; Baiker, A. *Langmuir* **2003**, *19*, 785–792.
- (9) Wirz, R.; Ferri, D.; Baiker, A. *Anal. Chem.* **2008**, *80*, 3572–3583.
- (10) Cass, Q. B.; Degani, A. L. G.; Tiritan, M. E.; Matlin, S. A.; Curran, D. P.; Balog, A. *Chirality* **1997**, *9*, 109–112.
- (11) Cass, Q. B.; Batigalhia, F. *J. Chromatogr. A* **2003**, *987*, 445–452.
- (12) Booth, T. D.; Lough, W. J.; Saeed, M.; Noctor, T. A. G.; Wainer, I. W. *Chirality* **1997**, *9*, 173–177.
- (13) Hu, Z. Q.; Jiang, J. W. *J. Phys. Chem. B* **2009**, *113*, 15851–15857.
- (14) Wang, T.; Chen, Y. D. W. *J. Chromatogr. A* **1999**, *855*, 411–421.
- (15) Wang, T.; Chen, Y. D. W.; Vailaya, A. *J. Chromatogr. A* **2000**, *902*, 345–355.

- (16) Wenslow, R. M.; Wang, T. *Anal. Chem.* **2001**, *73*, 4190–4195.
- (17) Wang, T.; Wenslow, R. M. *J. Chromatogr. A* **2003**, *1015*, 99–110.
- (18) Ma, S.; Shen, S.; Lee, H.; Eriksson, M.; Zeng, X.; Xu, J.; Fandrick, K.; Yee, N.; Senanayake, C.; Grinberg, N. *J. Chromatogr. A* **2009**, *1216*, 3784–3793.
- (19) Li, Y. Y.; Liu, D. H.; Wang, P.; Zhou, Z. Q. *J. Sep. Sci.* **2010**, *33*, 3245–3255.
- (20) Okamoto, Y.; Kaida, Y.; Hayashida, H.; Hatada, K. *Chem. Lett.* **1990**, *909*–912.
- (21) Muthupandi, P.; Alamsetti, S. K.; Sekar, G. *Chem. Commun.* **2009**, 3288–3290.
- (22) Zheng, J. R.; Kwak, K.; Chen, X.; Asbury, J. B.; Fayer, M. D. *J. Am. Chem. Soc.* **2006**, *128*, 2977–2987.
- (23) Zugenmaier, P.; Steinmeier, H. *Polymer* **1986**, *27*, 1601–1608.
- (24) Dauber-Osguthorpe, P.; Roberts, V. A.; Osguthorpe, D. J.; Wolff, J.; Genest, M.; Hagler, A. T. *Proteins: Struct., Funct., Genet.* **1988**, *4*, 31–47.
- (25) Nose, S. *Prog. Theor. Phys. Suppl.* **1991**, *1*–46.
- (26) Randhawa, H. S.; Rao, K. G.; Rao, C. N. R. *Spectrochim. Acta, Part A* **1974**, *A 30*, 1915–1922.
- (27) Maklakov, L. I.; Furer, A. L.; Furer, V. L.; Zhikhareva, N. A.; Alekseev, V. V. *J. Appl. Spectrosc.* **1981**, *34*, 6.
- (28) Bellamy, L. J. *The Infra-Red Spectra of Complex Molecules*, 3rd ed.; Wiley: New York, 1975.
- (29) Pawelka, Z.; Kryachko, E. S.; Zeegers-Huyskens, T. *Chem. Phys.* **2003**, *287*, 143–153.
- (30) Haisa, M.; Kashino, S.; Morimoto, M. *Acta Crystallogr. Sect. B: Struct. Commun.* **1980**, *36*, 2832–2834.